Power-Law Entanglement and Hilbert Space Fragmentation in Nonreciprocal Quantum Circuits

K. Klocke,[1] J. E. Moore,[1,2] and M. Buchhold[3]
[1]Department of Physics, University of California, Berkeley, California 94720, USA
[2]Materials Sciences Division, Lawrence Berkeley National Laboratory, Berkeley, California 94720, USA
[3]Institut für Theoretische Physik, Universität zu Köln, D-50937 Cologne, Germany

(Received 15 May 2024; accepted 16 July 2024; published 12 August 2024)

Quantum circuits utilizing measurement to evolve a quantum wave function offer a new and rich playground to engineer unconventional entanglement dynamics. Here, we introduce a hybrid, nonreciprocal setup featuring a quantum circuit, whose updates are conditioned on the state of a classical dynamical agent. In our example the circuit is represented by a Majorana quantum chain controlled by a classical N-state Potts chain undergoing pair flips. The local orientation of the classical spins controls whether randomly drawn local measurements on the quantum chain are allowed or not. This imposes a dynamical kinetic constraint on the entanglement growth, described by the transfer matrix of an N-colored loop model. It yields an equivalent description of the circuit by an $SU(N)$-symmetric Temperley-Lieb Hamiltonian or by a kinetically constrained surface growth model for an N-component height field. For $N = 2$, we find a diffusive growth of the half-chain entanglement toward a stationary profile $S(L) \sim L^{1/2}$ for L sites. For $N \geq 3$, the kinetic constraints impose Hilbert space fragmentation, yielding subdiffusive growth toward $S(L) \sim L^{0.57}$. This showcases how the control by a classical dynamical agent can enrich the entanglement dynamics in quantum circuits, paving a route toward novel entanglement dynamics in nonreciprocal hybrid circuit architectures.

DOI: 10.1103/PhysRevLett.133.070401

Introduction—Analog quantum circuits, incorporating unitary gates, midcircuit measurements, and quantum feedback, extend beyond traditional Hamiltonian or dissipative quantum systems. By utilizing measurement as a resource for irreversible quantum dynamics, quantum circuits offer a unique platform for shaping and manipulating entanglement. They enable applications such as quantum error correction [1–9], expedited state preparation, and the exploration of novel phenomena like measurement-induced entanglement transitions [10–23]. In particular, the efficient preparation of entanglement patterns associated to circuit analogs of topologically nontrivial or gapless ground states has recently attracted attention due to the challenge of preparing such states by exclusively using unitary operations [24–34].

Here, we propose a novel route to implement enriched entanglement dynamics: the nonreciprocal coupling of a quantum circuit to a classical dynamical agent. Nonreciprocity indicates that the evolution of the quantum circuit is influenced by the classical agent, but not vice versa. The dynamical agent evolves according to a set of predetermined update rules and typically implements a non-Markovian environment, which governs the buildup of entanglement. We consider a system composed of a Majorana quantum circuit conditioned on a classical spin chain undergoing pair-flip dynamics. Utilizing the loop model framework for Majorana circuits [35,36], we show that this circuit features both a dynamical fragmentation of the Hilbert space and an algebraic growth of the entanglement entropy $S(L) \sim L^{\alpha}$ familiar from $SU(N)$-symmetric quantum models such as, e.g., the Fredkin chain [37–40]. We validate this picture by extensive numerical simulations of the nonreciprocal circuit.

Majorana loop model circuits—We consider the dynamics of entanglement in Clifford circuits of L Majorana fermions $\{\gamma_l, \gamma_m\} = 2\delta_{l,m}$ on a one-dimensional chain with open boundary conditions. The evolution is generated by parity checks of bilinears $i\gamma_l\gamma_m$, yielding a stabilizer state $\rho = \prod_\alpha [(\mathbb{1} + i\gamma_{l_\alpha}\gamma_{m_\alpha})/2]$ with well-known parities $i\gamma_{l_\alpha}\gamma_{m_\alpha}$. The Majorana parity measurements considered here correspond to local Pauli measurements in qubit-based quantum devices. The state ρ admits a graphical representation via Majorana worldlines, each of which connects two Majorana fermions γ_l, γ_m with well-defined parity $i\gamma_l\gamma_m = \pm 1$ [18,19,35,36,41]. Performing a parity check $i\gamma_l\gamma_m = \pm 1$ acts with either the projector $\mathcal{P}_{l,m} = \frac{1}{2}(\mathbb{1} - i\gamma_l\gamma_m)$ or its sign-flipped partner $\mathcal{P}_{m,l}$ on ρ, thus rewiring the worldlines [see Fig. 1(a)]. The entanglement entropy of a subsystem A, $S_A = -\mathrm{Tr}[\rho_A \log_2(\rho_A)]$ is agnostic to the parity sign and only depends on the modulus $|\langle i\gamma_l\gamma_m \rangle|$. This has important consequences: both $\mathcal{P}_{l,m}, \mathcal{P}_{m,l}$ implement precisely the same change in entanglement, defining an

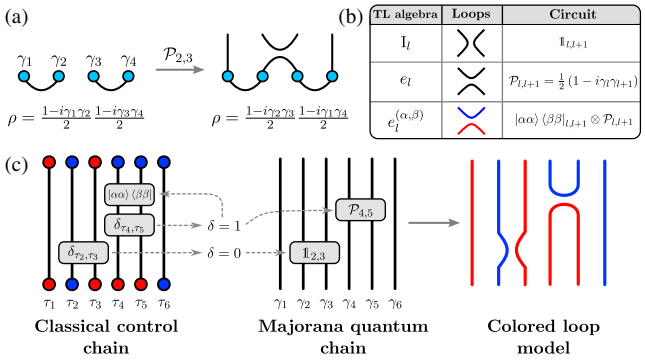

FIG. 1. Nonreciprocal circuit for colored loop models. (a) Diagrammatic representation of Majorana worldlines being rewired under projective measurement. (b) A dictionary relating the TL algebra elements to their loop representation and corresponding circuit operation. (c) Effective nonreciprocal circuit for the colored loop model. If and only if a brick $\{\tau_l, \tau_{l+1}, \gamma_l, \gamma_{l+1}\}$ has two identical Potts spins $\tau_l = \tau_{l+1}$ an update is performed: the parity $i\gamma_l\gamma_{l+1}$ is measured and the Potts spins are randomly flipped $\tau_l, \tau_{l+1} \to \beta$.

equivalence relation for projections $\mathcal{P}_{l,m} \sim \mathcal{P}_{m,l}$ such that circuits are elements of the Brauer algebra $\mathcal{B}_L(1)$ over L Majorana fermions [35].

For nearest-neighbor Majorana measurements, the fundamental generators of dynamics are projectors $e_l \equiv \mathcal{P}_{l,l+1}$. They obey the Temperley-Lieb (TL) algebra [42]

$$e_l^2 = n e_l, \qquad e_l e_{l\pm1} e_l = e_l, \tag{1}$$

describing loop models with fugacity n. Projective measurements exclusively implement $n = 1$. Depending on geometry and the set of measured operators, Majorana circuits with $n = 1$ realize a spectrum of phases and critical points [35,36,43–45], e.g., of (coupled) Potts models.

Colored loop models from nonreciprocal circuits—In order to further enrich the quantum dynamics in Majorana circuits and to reach beyond the $n = 1$ paradigm, we introduce a nonreciprocal circuit architecture implementing a *colored* TL algebra [46–48]. This algebra is generated by projectors $e_l^{(\alpha,\beta)}$ with fugacity $n = 1$ that are additionally decorated with N color degrees of freedom, α, β. The operators obey the algebra [49]

$$e_l^{(\alpha,\nu)} e_l^{(\nu',\beta)} = \delta_{\nu,\nu'} e_l^{(\alpha,\beta)}. \tag{2}$$

In the loop model framework, $e_l^{(\alpha,\beta)}$ closes a loop of color β and opens a new loop of color α; see Fig. 1(a). Averaging over all colors with equal probability yields the generators $E_l = \sum_{\alpha,\beta=1}^{N} e_l^{(\alpha,\beta)}$, which implement the (uncolored) TL algebra with fugacity N [50–52],

$$E_l^2 = N E_l, \qquad E_l E_{l\pm1} E_l = E_l. \tag{3}$$

Such a colored TL algebra arises, e.g., in the pair-flip model [53,54], where the color symmetry imposes kinetic constraints resulting in Hilbert space fragmentation and unconventional entanglement scaling in the ground state.

In order to implement the algebra in Eq. (2), we augment the quantum circuit of L Majorana fermions with a "control" chain of L classical N-state Potts spins $\tau_l \in \{1, \ldots, N\}$. The classical spins influence the evolution of the Majorana chain via a nonreciprocal interaction: At each time step t, a "brick" $\{\gamma_l, \gamma_{l+1}, \tau_l, \tau_{l+1}\}$ consisting of two adjacent Majorana fermions and two corresponding Potts spins is chosen randomly from all $L-1$ possible pairings (open boundary conditions). *If and only if* the two Potts spins have the same "color" ($\tau_l = \tau_{l+1} = \alpha$), two updates are performed: (i) the parity operator $i\gamma_l\gamma_{l+1}$ is measured; (ii) both Potts spins are flipped to a randomly and uniformly chosen color $\tau_l, \tau_{l+1} \to \beta \in \{1, \ldots, N\}$. This implements the generator of the colored TL algebra

$$e_l^{(\alpha,\beta)} = |\alpha\alpha\rangle\langle\beta\beta|_{l,l+1} \otimes \mathcal{P}_{l,l+1}. \tag{4}$$

The Potts spins thus decorate the Majorana worldlines, yielding a colored loop model for the effective dynamics.

Ensemble Hamiltonian—Let $\epsilon_{\alpha\beta}^{(l)} \in [0, 1]$ be the probability applying $e_l^{(\alpha,\beta)}$ site l in a unit time step. Averaging over all circuit trajectories then reproduces a loop ensemble generated by an effective transfer matrix T_l acting on each pair of neighboring sites as $T_l = \mathbb{1} + \epsilon_{\alpha\beta}^{(l)} e_l^{(\alpha,\beta)}$. This is exactly the transfer matrix arising from imaginary-time evolution with a Hamiltonian

$$H = \sum_l \sum_{\alpha,\beta} \epsilon_{\alpha\beta}^{(l)} e_l^{(\alpha,\beta)}. \tag{5}$$

Drawing the probabilities uniformly in space $\epsilon_{\alpha\beta}^{(l)} \equiv \epsilon_{\alpha\beta}$, Eq. (5) is the so-called pair-flip (PF) Hamiltonian. Choosing further identical transition rates $\epsilon_{\alpha\beta} \equiv \epsilon$ yields the TL Hamiltonian $H = \epsilon \sum_l E_l$. The transfer matrix picture elucidates that each trajectory of the random circuit represents an element of the stochastic series expansion for the partition function $\sim \exp(-\beta H)$ in the limit $\beta \to \infty$. The ensemble Hamiltonian thus is the Markov generator for a classical stochastic process that produces individual circuit trajectories (i.e., colored loop configurations) [55–57]. The statistical ensemble of wave functions produced by the circuit is identical to the ensemble that forms the quantum ground state of the Hamiltonian (5) by coherent superposition.

Symmetries and fragmentation—The TL generators $e_l^{(\alpha,\beta)}$ induce pair-flip dynamics that conserve $N-1$ independent $U(1)$ charges $Q_\alpha = \sum_l (-1)^l |\alpha\rangle\langle\alpha|_l$ [58,59]. Their presence implies a continuity equation yielding diffusive charge transport. The TL Hamiltonian maps exactly to the spin-1/2 Heisenberg chain for $N = 2$ and the spin-1

biquadratic chain $H_{N=3} = -\sum_l (\vec{S}_l \cdot \vec{S}_{l+1})^2$ for $N = 3$ [60–63], and the $U(1)^{N-1}$ symmetry is promoted to $SU(N)$. We note, however, that for the circuit, $SU(N)$ is a symmetry of the ensemble, not of individual trajectories. In addition to the global symmetries, there is an extensive number of additional conserved quantities, which for $N = 2$ can be attributed to integrability.

For $N \geq 3$, the TL and PF models are paradigmatic examples of strong Hilbert space fragmentation [54,59], with the largest Krylov sector comprising a measure-zero subset of the Hilbert space in the thermodynamic limit [53,59]. This separates $N \geq 3$ from $N = 2$: $N = 2$ has a commutant algebra of dimension $L + 1$ and thus fragmentation is absent. $N \geq 3$ gives an exponentially large commutant algebra of dimension $[(N-1)^{L+1} - 1]/(N-2)$. We thus expect transport and the buildup of entanglement to be slower (subdiffusive) for $N \geq 3$ compared to diffusion for $N = 2$.

A note on the nature of fragmentation: while the PF model with $N \geq 3$ displays fragmentation in a local product basis—referred to as "classically" fragmented—the TL model displays fragmentation in an entangled basis—referred to as "quantum" fragmented. In our setup, the Potts spins undergo a stochastic classical pair-flip dynamics, with the colors always in a product state. Even though the ensemble retains a statistical $SU(N)$ symmetry, the trajectory-level dynamics ought to reflect the classical fragmentation of the PF model. This fragmentation is imprinted upon the entangled quantum dynamics of the Majorana chain via the nonreciprocal interaction.

Surface growth models and universality—Besides the link to fragmented quantum Hamiltonians, the dynamics of Majorana worldlines is directly connected to the dynamics of height models describing surface growth. This grants access to dynamical scaling exponents governing the growth of entanglement in the circuit.

Consider a stabilizer state and its loop configuration in the uncolored Majorana chain. We define a height field $h_l = S_{[1,l]}$ as the entanglement entropy of the first l Majorana fermions. The height field satisfies the boundary conditions $h_0 = h_L = 0$ and the restricted solid-on-solid constraint $h_{l+1} - h_l = \pm 1$. Edges connecting adjacent heights then define a Dyck path [56,57] (i.e., one with $h_l \geq 0$), for which left (right) ends of loops correspond to an increase (decrease) in the height, see Fig. 2.

A projective measurement $\mathcal{P}_{l,l+1}$ then implements one of the following two processes: (i) single-site adsorption [Fig. 2(a)] or (ii) a desorption avalanche [Fig. 2(b)]. Adsorption converts a local minimum $\{\ldots, h, h-1, h, \ldots\}$ to a local maximum $\{\ldots, h, h+1, h, \ldots\}$, increasing entanglement locally across a cut. Desorption occurs when measurement acts on a region of constant slope in the height field (e.g., $\{\ldots, h-1, h, h+1, \ldots\}$), corresponding to two nested loops, e.g., the two red loops in Fig. 2(b). Desorption is disentangling and may cause a nonlocal

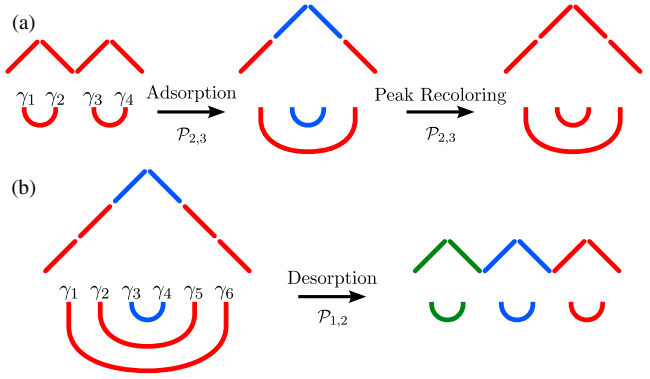

FIG. 2. Height model and Dyck path representation of the colored circuit. Given a loop configuration, the corresponding Dyck path is defined by increasing (decreasing) the path height at the left (right) end of a loop. Measurement implements one of the following operations on the height field. (a) At a local minimum, measurement (here of $i\gamma_2\gamma_3$) implements single-site adsorption, wherein the local height increases. At a local maximum, measurement can recolor the peak of the path. (b) Otherwise, measurements trigger a desorption avalanche (here we measure $i\gamma_1\gamma_2$), wherein the height is decreased in the whole region between the endpoints of the loop acted upon (i.e., the region between γ_2, γ_5).

"avalanche" wherein the whole region enclosed by the inner loop has its height reduced by two since the two previously nested loops no longer cross the intervening region.

The colored loop model in the nonreciprocal circuit then yields colored Dyck paths, where the edge connecting h_l and h_{l+1} has the color given by τ_l. This coloring imposes a kinetic constraint such that adsorption and desorption can occur only when adjacent edges in the Dyck path have the same color. Moreover, we now have a third process wherein local maxima can be recolored without changing the heights [see Fig. 2(a)].

Surface growth models describing a height field h_l give rise to Family-Vicsek scaling $f(L,t) = L^{\alpha} F(tL^{-z})$ for quantities $f(L,t)$ related to surface roughness [64–68]. The scaling function $F(x)$ grows algebraically as x^{β} for small argument and approaches a constant for $x \gg 1$. The growth exponent β is related to the roughness exponent α and the dynamical exponent z via $\beta = \alpha/z$. The relation to surface growth provides lower bounds on the height field h_l, i.e., the entanglement growth, and estimates for the universal scaling exponents.

Entanglement bounds from surface growth—The color dynamics on the control chain is reversible, yielding detailed balance and a uniform distribution over states in the accessible Krylov sector. The largest Krylov sector in the classical chain yields Dyck paths with the average height growing as $\sqrt{L}$ for all N [53]. However, for a purely classical chain, i.e., without the Majorana worldlines in the quantum chain, the mapping between Dyck paths and color

configurations is not unique. For example, the color configuration $|1111\rangle$ might arise in two different loop configurations shown in Fig. 2(a). In Ref. [53] each color configuration is mapped to the Dyck path with the smallest possible height, providing a lower bound of $\sqrt{L}$ for the height field and the entanglement entropy.

Critical exponents from surface growth—For $N = 2$, the TL Hamiltonian (5) corresponds to the spin-1/2 Heisenberg chain, which is a Markov generator for the symmetric simple exclusion process [69–72]. The dynamics of the symmetric simple exclusion process lie in the Edwards-Wilkinson (EW) universality class, with exponents $z = 2$, $\alpha = \frac{1}{2}$ and $\beta = \frac{1}{4}$ [69–71,73–75]. For $N \geq 3$, Hilbert space fragmentation will modify the critical exponents compared to $N = 2$. The dynamics of the Hamiltonian (5) with $N = 3$ has been explored in the context of classical deposition-evaporation models for colored dimers and trimers, where numerical results show subdiffusion with exponent $z \approx 2.5$ and growth exponent $\beta \approx 0.19$ [77–80]. More recent studies on dynamics in the Fredkin chain, which admits a closely related description in terms of kinetically constrained surface growth, yield a dynamical exponent $z \approx 2.7$ in the zero magnetization sector [63,81,82].

Dynamics of entanglement—We simulate the growth of entanglement in the nonreciprocal circuit, starting from an initial state with uniform coloring $\tau_l = 1$ and local pairing $\langle i\gamma_{2l-1}\gamma_{2l}\rangle = 1$. This corresponds to a "flat" height configuration, lying in the largest Krylov sector, where each loop has a well-defined color.

We provide detailed simulation results of both $N = 2$ and $N = 3$ colors. Here, $N = 3$ is a representative for generic $N \geq 3$, while $N = 2$ is special since it has distinct symmetries and no Hilbert space fragmentation. In general for $N \geq 2$ we observe an algebraic growth of the entanglement entropy with time, $S_{L/2}(t) \sim t^{\beta_N}$, as shown in Fig. 3(a). For the growth exponent β_N, we find $\beta_2 = 0.246 \pm 0.002$ for $N = 2$ [83], consistent with the expected value of $\beta_2 = 1/4$ arising from the EW universality class. By contrast, for $N \geq 3$ we observe slower growth of the entanglement with $\beta_3 = 0.206 \pm 0.004$, comparable to the growth exponent found in the colored dimer deposition-evaporation model.

We assume Family-Vicsek scaling for the entanglement growth, yielding $S_{L/2}(t) \sim L^{\alpha} f(tL^{-z})$, to first extract the dynamical critical exponent z independent of α by a scaling collapse analysis for an ansatz $S_{L/2}(t) = S_{L/2}(t \to \infty)$ $f(tL^{-z})$, shown in Fig. 3(b). For $N = 2$, we observe diffusive dynamics with $z = 2.00 \pm 0.02$ as expected. With more colors, we instead find subdiffusive behavior, with $N = 3$ giving $z = 2.65 \pm 0.06$. This value is consistent with the dynamical exponent in the Fredkin chain [63,81,82] and dimer models [77–80].

Steady-state entanglement scaling—After a time $t \sim L^z$, the average entanglement entropy saturates to a subextensive value that scales algebraically in system size as $S_\ell(t \to \infty) \sim (\ell(L-\ell)/L)^{\alpha_N}$. In Fig. 4, we show the scaling of $S_{L/2}$ with respect to L as well as the data collapse of the full entanglement profile S_ℓ. For $N = 2$, we find $\alpha_2 = 0.506 \pm 0.003$, consistent with the expected EW

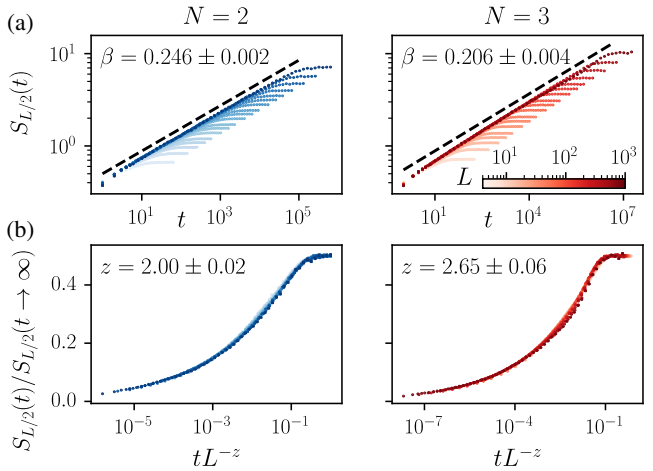

FIG. 3. Growth of the half-chain entanglement entropy beginning from a trivial initial state for $N = 2$ (left) and $N = 3$ (right). (a) We observe an algebraic scaling $S_{L/2}(t) \sim t^{\beta_N}$, where the growth exponent is $\beta_2 = 0.246 \pm 0.002$ and $\beta_3 = 0.206 \pm 0.004$. (b) Rescaling of time yields a data collapse of the normalized entanglement entropy $S_{L/2}(t)/S_{L/2}(t \to \infty)$. For $N = 2$ we find dynamical exponent $z = 2.00 \pm 0.02$, while for $N = 3$ we find $z = 2.65 \pm 0.06$.

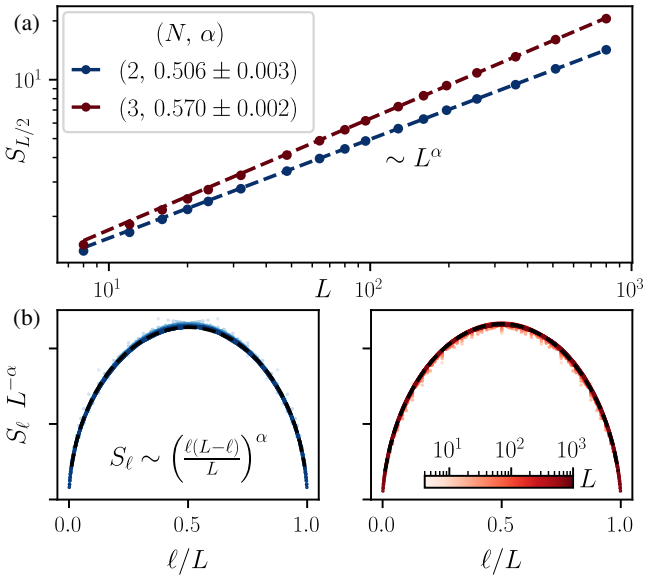

FIG. 4. (a) Algebraic scaling of the steady-state half-chain entanglement entropy $S_{L/2} \sim L^{\alpha}$ for $N = 2, 3$ colors. With $N = 2$ (blue), we find $\alpha = 0.506 \pm 0.003$, while for $N = 3$ (red) we instead find $\alpha = 0.570 \pm 0.002$. (b) Data collapse of the entanglement profile S_ℓ confirms scaling of the form $S_\ell \sim (\ell(L-\ell)/L)^{\alpha}$ (black dashed lines).

universality. With more colors, $N \geq 3$, we observe a slightly larger exponent $\alpha_3 = 0.570 \pm 0.002$. Both values of α_N are consistent with that predicted by the dynamical scaling relation $\alpha = z\beta$. Nonetheless, it is surprising to find $\alpha_3 > \frac{1}{2}$, as one might expect $\alpha = \frac{1}{2}$ from previous numerical studies and the height distribution arising in the Dyck path ensemble.

The algebraic scaling of entanglement found here is *robust* so long as the color symmetry is preserved. For example, dimerization of the measurement probability is a relevant perturbation in the $N = 1$ limit, driving the system into one of two topologically distinct area-law phases. In the colored loop ensemble with $N \geq 2$, however, such dimerization fails to alleviate the kinetic constraints, instead it only renormalizes the effective diffusion constant (or timescale for $N \geq 3$).

Discussion—We have introduced a nonreciprocal quantum circuit realizing the colored Temperley-Lieb algebra, for which symmetries and kinetic constraints of the classical dynamics are imprinted upon the quantum chain. This leads to robust power-law entanglement scaling and distinct dynamical exponents. Similar ideas can emerge in purely unitary random [54] and Floquet [84] circuits, where kinetic constraints modify ergodicity and thermalization time scales. More generally, we may consider coupling a stochastic classical cellular automaton on the control chain to the measurement dynamics on the quantum chain, yielding a broader family of entanglement dynamics and related surface-growth models. A further step, enabled by spacetime locality of the interaction would be to promote the classical "control" chain to a quantum system, yielding a strictly quantum circuit. For example, with $N = 2$ we may promote the Potts spins to a chain of qubits where σ^z_l encodes the "color." Then projective measurement of $\sigma^z_l \sigma^z_{l+1}$ determines whether or not two adjacent spins have the same color.

An implementation of the reciprocal circuit can be envisioned for current quantum computing platforms with high fidelity midcircuit measurements in the computational basis, including trapped ions [2,85,86], neutral atom arrays [6,7,9,87–89], and superconducting qubits [90]. Here, $2L$ Majorana fermions arise from a Jordan-Wigner transformation of an L-qubit array, i.e., by translating the nearest-neighbor fermionic parities to qubit operators $i\gamma_{2l}\gamma_{2l+1} \to \sigma^x_l \sigma^x_{l+1}$ and $i\gamma_{2l-1}\gamma_{2l} \to \sigma^z_l$, projective measurements of which are available [1,2,4,5].

Acknowledgments—K. K. was primarily supported by an NSF Graduate Fellowship under Grant No. DGE 2146752. K. K. and J. E. M. acknowledge support from the U.S. Department of Energy, Office of Science, National Quantum Information Science Research Centers, Quantum Science Center. J. E. M. acknowledges support from a Simons Investigatorship. M. B. acknowledges support from the Deutsche Forschungsgemeinschaft (DFG, German Research Foundation) under Germany's Excellence Strategy Cluster of Excellence Matter and Light for Quantum Computing (ML4Q) EXC 2004/1 390534769, and by the DFG Collaborative Research Center (CRC) 183 Project No. 277101999 -project B02.

[1] R. Stricker, D. Vodola, A. Erhard, L. Postler, M. Meth, M. Ringbauer, P. Schindler, T. Monz, M. Müller, and R. Blatt, Experimental deterministic correction of qubit loss, Nature (London) **585**, 207 (2020).

[2] C. Ryan-Anderson, J. G. Bohnet, K. Lee, D. Gresh, A. Hankin, J. P. Gaebler, D. Francois, A. Chernoguzov, D. Lucchetti, N. C. Brown, T. M. Gatterman, S. K. Halit, K. Gilmore, J. A. Gerber, B. Neyenhuis, D. Hayes, and R. P. Stutz, Realization of real-time fault-tolerant quantum error correction, Phys. Rev. X **11**, 041058 (2021).

[3] A. Erhard, H. Poulsen Nautrup, M. Meth, L. Postler, R. Stricker, M. Stadler, V. Negnevitsky, M. Ringbauer, P. Schindler, H. J. Briegel, R. Blatt, N. Friis, and T. Monz, Entangling logical qubits with lattice surgery, Nature (London) **589**, 220 (2021).

[4] S. Krinner, N. Lacroix, A. Remm, A. Di Paolo, E. Genois, C. Leroux, C. Hellings, S. Lazar, F. Swiadek, J. Herrmann, G. J. Norris, C. K. Andersen, M. Müller, A. Blais, C. Eichler, and A. Wallraff, Realizing repeated quantum error correction in a distance-three surface code, Nature (London) **605**, 669 (2022).

[5] W. P. Livingston, M. S. Blok, E. Flurin, J. Dressel, A. N. Jordan, and I. Siddiqi, Experimental demonstration of continuous quantum error correction, Nat. Commun. **13**, 2307 (2022).

[6] D. Bluvstein *et al.*, Logical quantum processor based on reconfigurable atom arrays, Nature (London) **626**, 58 (2023).

[7] M. A. Norcia *et al.*, Midcircuit qubit measurement and rearrangement in a ^{171}Yb atomic array, Phys. Rev. X **13**, 041034 (2023).

[8] S. Ma, G. Liu, P. Peng, B. Zhang, S. Jandura, J. Claes, A. P. Burgers, G. Pupillo, S. Puri, and J. D. Thompson, High-fidelity gates and mid-circuit erasure conversion in an atomic qubit, Nature (London) **622**, 279 (2023).

[9] K. Singh, C. E. Bradley, S. Anand, V. Ramesh, R. White, and H. Bernien, Mid-circuit correction of correlated phase errors using an array of spectator qubits, Science **380**, 1265 (2023).

[10] Y. Li, X. Chen, and M. P. A. Fisher, Measurement-driven entanglement transition in hybrid quantum circuits, Phys. Rev. B **100**, 134306 (2019).

[11] B. Skinner, J. Ruhman, and A. Nahum, Measurement-induced phase transitions in the dynamics of entanglement, Phys. Rev. X **9**, 031009 (2019).

[12] S. Choi, Y. Bao, X.-L. Qi, and E. Altman, Quantum error correction in scrambling dynamics and measurement-induced phase transition, Phys. Rev. Lett. **125**, 030505 (2020).

[13] Y. Bao, S. Choi, and E. Altman, Theory of the phase transition in random unitary circuits with measurements, Phys. Rev. B **101**, 104301 (2020).

[14] M. Buchhold, Y. Minoguchi, A. Altland, and S. Diehl, Effective theory for the measurement-induced phase transition of Dirac fermions, Phys. Rev. X **11**, 041004 (2021).
[15] Y. Li, R. Vasseur, M. P. A. Fisher, and A. W. W. Ludwig, Statistical mechanics model for Clifford random tensor networks and monitored quantum circuits, Phys. Rev. B **109**, 174307 (2024).
[16] Y. Li, X. Chen, A. W. W. Ludwig, and M. P. A. Fisher, Conformal invariance and quantum nonlocality in critical hybrid circuits, Phys. Rev. B **104**, 104305 (2021).
[17] M. Ippoliti, M. J. Gullans, S. Gopalakrishnan, D. A. Huse, and V. Khemani, Entanglement phase transitions in measurement-only dynamics, Phys. Rev. X **11**, 011030 (2021).
[18] S. Sang and T. H. Hsieh, Measurement-protected quantum phases, Phys. Rev. Res. **3**, 023200 (2021).
[19] S. Sang, Y. Li, T. Zhou, X. Chen, T. H. Hsieh, and M. P. A. Fisher, Entanglement negativity at measurement-induced criticality, PRX Quantum **2**, 030313 (2021).
[20] T. Müller, S. Diehl, and M. Buchhold, Measurement-induced dark state phase transitions in long-ranged fermion systems, Phys. Rev. Lett. **128**, 010605 (2022).
[21] C. Noel, P. Niroula, D. Zhu, A. Risinger, L. Egan, D. Biswas, M. Cetina, A. V. Gorshkov, M. J. Gullans, D. A. Huse, and C. Monroe, Measurement-induced quantum phases realized in a trapped-ion quantum computer, Nat. Phys. **18**, 760 (2022).
[22] M. P. Fisher, V. Khemani, A. Nahum, and S. Vijay, Random quantum circuits, Annu. Rev. Condens. Matter Phys. **14**, 335 (2023).
[23] E. Chertkov, Z. Cheng, A. C. Potter, S. Gopalakrishnan, T. M. Gatterman, J. A. Gerber, K. Gilmore, D. Gresh, A. Hall, A. Hankin, M. Matheny, T. Mengle, D. Hayes, B. Neyenhuis, R. Stutz, and M. Foss-Feig, Characterizing a non-equilibrium phase transition on a quantum computer, Nat. Phys. **19**, 1799 (2023).
[24] L. Piroli, G. Styliaris, and J. I. Cirac, Quantum circuits assisted by local operations and classical communication: Transformations and phases of matter, Phys. Rev. Lett. **127**, 220503 (2021).
[25] S. Bravyi, I. Kim, A. Kliesch, and R. Koenig, Adaptive constant-depth circuits for manipulating non-Abelian anyons, arXiv:2205.01933.
[26] N. Tantivasadakarn, R. Thorngren, A. Vishwanath, and R. Verresen, Long-range entanglement from measuring symmetry-protected topological phases, Phys. Rev. X **14**, 021040 (2024).
[27] R. Verresen, N. Tantivasadakarn, and A. Vishwanath, Efficiently preparing Schrödinger's cat, fractons and non-Abelian topological order in quantum devices, arXiv:2112.03061.
[28] T.-C. Lu, L. A. Lessa, I. H. Kim, and T. H. Hsieh, Measurement as a shortcut to long-range entangled quantum matter, PRX Quantum **3**, 040337 (2022).
[29] M. Foss-Feig, A. Tikku, T.-C. Lu, K. Mayer, M. Iqbal, T. M. Gatterman, J. A. Gerber, K. Gilmore, D. Gresh, A. Hankin, N. Hewitt, C. V. Horst, M. Matheny, T. Mengle, B. Neyenhuis, H. Dreyer, D. Hayes, T. H. Hsieh, and I. H. Kim, Experimental demonstration of the advantage of adaptive quantum circuits, arXiv:2302.03029.
[30] M. Iqbal, N. Tantivasadakarn, T. M. Gatterman, J. A. Gerber, K. Gilmore, D. Gresh, A. Hankin, N. Hewitt, C. V. Horst, M. Matheny, T. Mengle, B. Neyenhuis, A. Vishwanath, M. Foss-Feig, R. Verresen, and H. Dreyer, Topological order from measurements and feed-forward on a trapped ion quantum computer, arXiv:2302.01917.
[31] N. Tantivasadakarn, A. Vishwanath, and R. Verresen, Hierarchy of topological order from finite-depth unitaries, measurement, and feedforward, PRX Quantum **4**, 020339 (2023).
[32] N. Tantivasadakarn, R. Verresen, and A. Vishwanath, Shortest route to non-Abelian topological order on a quantum processor, Phys. Rev. Lett. **131**, 060405 (2023).
[33] T.-C. Lu, Z. Zhang, S. Vijay, and T. H. Hsieh, Mixed-state long-range order and criticality from measurement and feedback, PRX Quantum **4**, 030318 (2023).
[34] M. Iqbal, N. Tantivasadakarn, R. Verresen, S. L. Campbell, J. M. Dreiling, C. Figgatt, J. P. Gaebler, J. Johansen, M. Mills, S. A. Moses, J. M. Pino, A. Ransford, M. Rowe, P. Siegfried, R. P. Stutz, M. Foss-Feig, A. Vishwanath, and H. Dreyer, Non-Abelian topological order and anyons on a trapped-ion processor, Nature (London) **626**, 505 (2024).
[35] K. Klocke and M. Buchhold, Majorana loop models for measurement-only quantum circuits, Phys. Rev. X **13**, 041028 (2023).
[36] A. Nahum and B. Skinner, Entanglement and dynamics of diffusion-annihilation processes with Majorana defects, Phys. Rev. Res. **2**, 023288 (2020).
[37] S. Bravyi, L. Caha, R. Movassagh, D. Nagaj, and P. W. Shor, Criticality without frustration for quantum spin-1 chains, Phys. Rev. Lett. **109**, 207202 (2012).
[38] O. Salberger and V. Korepin, Fredkin spin chain, arXiv:1605.03842.
[39] R. Movassagh and P. W. Shor, Supercritical entanglement in local systems: Counterexample to the area law for quantum matter, Proc. Natl. Acad. Sci. U.S.A. **113**, 13278 (2016).
[40] R. Movassagh, Entanglement and correlation functions of the quantum Motzkin spin-chain, J. Math. Phys. (N.Y.) **58**, 031901 (2017).
[41] J. Merritt and L. Fidkowski, Entanglement transitions with free fermions, Phys. Rev. B **107**, 064303 (2023).
[42] Including the normalization of the wave function after each projection.
[43] N. Lang and H. P. Büchler, Entanglement transition in the projective transverse field Ising model, Phys. Rev. B **102**, 094204 (2020).
[44] Y. Li and M. P. A. Fisher, Decodable hybrid dynamics of open quantum systems with $\mathbb{z}_2$ symmetry, Phys. Rev. B **108**, 214302 (2023).
[45] F. Roser, H. P. Büchler, and N. Lang, Decoding the projective transverse field Ising model, Phys. Rev. B **107**, 214201 (2023).
[46] U. Grimm and P. A. Pearce, Multi-colour braid-monoid algebras, J. Phys. A **26**, 7435 (1993).
[47] U. Grimm and P. P. Martin, The bubble algebra: Structure of a two-colour Temperley–Lieb algebra, J. Phys. A **36**, 10551 (2003).
[48] U. Grimm and S. O. Warnaar, Yang-Baxter algebras based on the two-colour BWM algebra, J. Phys. A **28**, 7197 (1995).

[49] Technically speaking there is also a second relation like in Eq. (1) corresponding to ambient isotopy of colored loops. It is $e_l^{(\alpha,\nu)} e_{l\pm1}^{(\nu,\nu)} e_l^{(\nu,\beta)} = e_l^{(\alpha,\beta)} P_{l\pm1}^{\nu}$, where P_l^{ν} is a projector on the color degree of freedom on the corresponding worldline.

[50] A. Nahum, J. T. Chalker, P. Serna, M. Ortuño, and A. M. Somoza, Phase transitions in three-dimensional loop models and the CP^{n-1} sigma model, Phys. Rev. B **88**, 134411 (2013).

[51] R. K. Kaul, R. G. Melko, and A. W. Sandvik, Bridging lattice-scale physics and continuum field theory with quantum Monte Carlo simulations, Annu. Rev. Condens. Matter Phys. **4**, 179 (2013).

[52] H. G. Evertz, The loop algorithm, Adv. Phys. **52**, 1 (2003).

[53] L. Caha and D. Nagaj, The pair-flip model: A very entangled translationally invariant spin chain, arXiv:1805.07168.

[54] Y. Han, X. Chen, and E. Lake, Exponentially slow thermalization and the robustness of Hilbert space fragmentation, arXiv:2401.11294.

[55] P. A. Pearce, V. Rittenberg, J. d. Gier, and B. Nienhuis, Temperley-Lieb stochastic processes, J. Phys. A **35**, L661 (2002).

[56] J. de Gier, Loops, matchings and alternating-sign matrices, arXiv:math/0211285.

[57] P. Zinn-Justin, Six-vertex, loop and tiling models: Integrability and combinatorics, arXiv:0901.0665.

[58] O. Hart, Exact Mazur bounds in the pair-flip model and beyond, arXiv:2308.00738.

[59] S. Moudgalya, A. Prem, D. A. Huse, and A. Chan, Spectral statistics in constrained many-body quantum chaotic systems, Phys. Rev. Res. **3**, 023176 (2021).

[60] A. Klümper, New results for q-state vertex models and the pure biquadratic spin-1 Hamiltonian, Europhys. Lett. **9**, 815 (1989).

[61] J. B. Parkinson, The $S = 1$ quantum spin chain with pure biquadratic exchange, J. Phys. C **21**, 3793 (1988).

[62] M. N. Barber and M. T. Batchelor, Spectrum of the biquadratic spin-1 antiferromagnetic chain, Phys. Rev. B **40**, 4621 (1989).

[63] X. Chen, E. Fradkin, and W. Witczak-Krempa, Gapless quantum spin chains: Multiple dynamics and conformal wavefunctions, J. Phys. A **50**, 464002 (2017).

[64] T. Vicsek and F. Family, Dynamic scaling for aggregation of clusters, Phys. Rev. Lett. **52**, 1669 (1984).

[65] F. Family and T. Vicsek, Scaling of the active zone in the Eden process on percolation networks and the ballistic deposition model, J. Phys. A **18**, L75 (1985).

[66] K. Fujimoto, R. Hamazaki, and Y. Kawaguchi, Family-Vicsek scaling of roughness growth in a strongly interacting Bose gas, Phys. Rev. Lett. **124**, 210604 (2020).

[67] K. Fujimoto, R. Hamazaki, and Y. Kawaguchi, Dynamical scaling of surface roughness and entanglement entropy in disordered fermion models, Phys. Rev. Lett. **127**, 090601 (2021).

[68] K. Fujimoto, R. Hamazaki, and Y. Kawaguchi, Impact of dissipation on universal fluctuation dynamics in open quantum systems, Phys. Rev. Lett. **129**, 110403 (2022).

[69] D. Kandel, E. Domany, and B. Nienhuis, A six-vertex model as a diffusion problem: Derivation of correlation functions, J. Phys. A **23**, L755 (1990).

[70] L.-H. Gwa and H. Spohn, Six-vertex model, roughened surfaces, and an asymmetric spin Hamiltonian, Phys. Rev. Lett. **68**, 725 (1992).

[71] D. Kim, Bethe ansatz solution for crossover scaling functions of the asymmetric XXZ chain and the Kardar-Parisi-Zhang-type growth model, Phys. Rev. E **52**, 3512 (1995).

[72] J. Neergaard and M. den Nijs, Crossover scaling functions in one dimensional dynamic growth models, Phys. Rev. Lett. **74**, 730 (1995).

[73] S. F. Edwards and D. R. Wilkinson, The surface statistics of a granular aggregate, Proc. R. Soc. A **381**, 17 (1982).

[74] L.-H. Gwa and H. Spohn, Bethe solution for the dynamical-scaling exponent of the noisy Burgers equation, Phys. Rev. A **46**, 844 (1992).

[75] By contrast, the asymmetric simple exclusion process exhibits Kardar-Parisi-Zhang dynamics. Tuning away from the symmetric point requires conditioning the measurement rates on the local height profile, akin to the unitary dynamics in Ref. [76]. However, the local Potts configuration does *not* confer information about the height field, thereby protecting the EW universality expected for our circuit with $N = 2$.

[76] R. Morral-Yepes, A. Smith, S. L. Sondhi, and F. Pollmann, Entanglement transitions in unitary circuit games, PRX Quantum **5**, 010309 (2024).

[77] H. M. Koduvely and D. Dhar, A model of subdiffusive interface dynamics with a local conservation of minimum height, J. Stat. Phys. **90**, 57 (1998).

[78] M. K. H. Menon and D. Dhar, The irreducible string and an infinity of additional constants of motion in a deposition-evaporation model on a line, J. Phys. A **28**, 6517 (1995).

[79] G. I. Menon, M. Barma, and D. Dhar, Conservation laws and integrability of a one-dimensional model of diffusing dimers, J. Stat. Phys. **86**, 1237 (1997).

[80] M. Barma and D. Dhar, Slow relaxation in a model with many conservation laws: Deposition and evaporation of trimers on a line, Phys. Rev. Lett. **73**, 2135 (1994).

[81] H. Singh, B. A. Ware, R. Vasseur, and A. J. Friedman, Subdiffusion and many-body quantum chaos with kinetic constraints, Phys. Rev. Lett. **127**, 230602 (2021).

[82] K. Adhikari and K. S. D. Beach, Slow dynamics of the Fredkin spin chain, Phys. Rev. B **104**, 115149 (2021).

[83] The reported values of β_N are obtained by fitting a power law to the dynamics $S_{L/2}(t)$ over the growth regime $1 \ll t \ll L^z$. The lower bound is taken to exclude transient initial state dependence, while the upper bound is taken to exclude late time saturation of the entanglement entropy. For $N = 2$ we take a window $20 < t < 0.1L^z$, and for $N = 3$ we take $100 < t < 0.03L^z$. The uncertainty is estimated from the fit uncertainty and further validated by (i) extrapolating to the thermodynamic limit and (ii) varying the upper and lower bounds for the fitted data range. Similarly, the roughness exponent α_N is determined by fitting a power law to the half-chain entanglement entropy $S_{L/2}$ in the steady state ($t \gg L^z$) for system sizes $L > L_0$. We fix $L_0 = 100$, for which the fitted exponent is well converged, and determine the uncertainty from the fit. Lastly, we determine the dynamical exponent z_N by scaling collapse of the normalized entanglement entropy dynamics $S_{L/2}(t)/S_{L/2}(t \to \infty)$. In particular, we fit a cubic B-spline

and minimize a squared residuals cost function. The uncertainty in z is estimated by the interval over which the cost function increases fourfold relative to the minimum.

[84] C. M. Langlett and S. Xu, Hilbert space fragmentation and exact scars of generalized Fredkin spin chains, Phys. Rev. B **103**, L220304 (2021).

[85] J. P. Gaebler, C. H. Baldwin, S. A. Moses, J. M. Dreiling, C. Figgatt, M. Foss-Feig, D. Hayes, and J. M. Pino, Suppression of midcircuit measurement crosstalk errors with micromotion, Phys. Rev. A **104**, 062440 (2021).

[86] S. A. Moses *et al.*, A race-track trapped-ion quantum processor, Phys. Rev. X **13**, 041052 (2023).

[87] E. Deist, Y.-H. Lu, J. Ho, M. K. Pasha, J. Zeiher, Z. Yan, and D. M. Stamper-Kurn, Mid-circuit cavity measurement in a neutral atom array, Phys. Rev. Lett. **129**, 203602 (2022).

[88] T. M. Graham, L. Phuttitarn, R. Chinnarasu, Y. Song, C. Poole, K. Jooya, J. Scott, A. Scott, P. Eichler, and M. Saffman, Midcircuit measurements on a single-species neutral alkali atom quantum processor, Phys. Rev. X **13**, 041051 (2023).

[89] J. W. Lis, A. Senoo, W. F. McGrew, F. Rönchen, A. Jenkins, and A. M. Kaufman, Midcircuit operations using the omg architecture in neutral atom arrays, Phys. Rev. X **13**, 041035 (2023).

[90] Y. Xu, G. Huang, N. Fruitwala, A. Rajagopala, R. K. Naik, K. Nowrouzi, D. I. Santiago, and I. Siddiqi, QubiC 2.0: An extensible open-source qubit control system capable of mid-circuit measurement and feed-forward, arXiv:2309.10333.